

# Investigating AAK1- and GAK-regulated virus-host interactions uncovers broad-spectrum antivirals

**Authors:** Elena Bekerman<sup>1†</sup>, Gregory Neveu<sup>1†,a</sup>, Ana Shulla<sup>2</sup>, Jennifer Brannan<sup>3</sup>, Szu-Yuan Pu<sup>1</sup>, Stanley Wang<sup>1</sup>, Fei Xiao<sup>1</sup>, Rina Barouch-Bentov<sup>1</sup>, Russell R. Bakken<sup>3</sup>, Roberto Mateo<sup>4</sup>, Jennifer Govero<sup>5</sup>, Claude M. Nagamine<sup>7</sup>, Michael S. Diamond<sup>5</sup>, Steven De Jonghe<sup>6</sup>, Piet Herdewijn<sup>6</sup>, John M. Dye<sup>3</sup>, Glenn Randall<sup>2</sup>, and Shirit Einav<sup>1\*</sup>

## Affiliations:

<sup>1</sup>Department of Medicine, Division of Infectious Diseases and Geographic Medicine, and Department of Microbiology and Immunology, Stanford University School of Medicine, Stanford, California, USA.

<sup>2</sup>Department of Microbiology, The University of Chicago, Chicago, Illinois, USA.

<sup>3</sup>US Army Medical Research Institute of Infectious Diseases, Viral Immunology Branch, Frederick, Fort Detrick, Maryland, USA.

<sup>4</sup>Department of Genetics and of Microbiology and Immunology, Stanford University School of Medicine, Stanford, California, USA.

<sup>5</sup>Departments of Medicine, Molecular Microbiology, and Pathology and Immunology, Washington University School of Medicine, St Louis, Missouri, USA.

<sup>6</sup>Laboratory of Medicinal Chemistry, Rega Institute for Medical Research, KU Leuven, Belgium.

<sup>7</sup>Department of Comparative Medicine, Stanford University School of Medicine, Stanford, California, USA.

<sup>a</sup> International Center for Infectiology Research, Université de Lyon; Inserm, U1111; Ecole Normale Supérieure de Lyon; Université Claude Bernard Lyon 1, Centre International de Recherche en Infectiologie; LabEx Ecofect, Université de Lyon, Lyon, France.

\*Address correspondence to: Shirit Einav, Department of Medicine, Stanford University, 300 Pasteur Drive, Lane building L127, Stanford, CA, 94305, USA. Phone: 650.723.8656; E-mail: seinav@stanford.edu.

† These authors contributed equally to this work.

The authors have declared that no conflict of interest exists.

**Abstract**

Global health is threatened by emerging viral infections, which largely lack effective vaccines or therapies. Targeting host pathways exploited by multiple viruses could offer broad-spectrum solutions. We previously reported that AAK1 and GAK, kinase regulators of the host adaptor proteins, AP1 and AP2, are essential for hepatitis C virus (HCV) infection, but the underlying mechanism and relevance to other viruses or in vivo infections remained unknown. Here, we discovered that AP1 and AP2 co-traffic with HCV particles in live cells. Moreover, we found that AAK1 and GAK are exploited during entry and infectious virus production of multiple viruses, including dengue and Ebola. Treatment with sunitinib and erlotinib, approved anticancer drugs with anti-AAK1 or GAK activity, or novel, more selective compounds inhibited intracellular HCV trafficking and multiple unrelated RNA viruses in culture with a high barrier to resistance. In murine models of dengue and Ebola infection, sunitinib/erlotinib combination protected against morbidity and mortality. We validated inhibition of AAK1 and GAK activity as an important mechanism of antiviral action by sunitinib and erlotinib and revealed potential roles for additional kinase targets. These findings advance our understanding of virus-host interactions and establish a proof-of-principle of a repurposed, host-targeted, approach to combat emerging viruses.

## Introduction

A major threat to human health is posed by emerging viruses, such as dengue (DENV) and Ebola (EBOV). Dengue is estimated to infect 390 million people annually in over 100 countries (1). Dengue fever can progress to a life-threatening disease, known as severe dengue, particularly upon a secondary infection with a heterologous DENV strain. Consequently, development of a dengue vaccine has been hampered by the necessity to generate simultaneous protection against four distinct DENV serotypes (2). As a further challenge, recent studies have suggested that pre-existing DENV immunity may enhance Zika virus (ZIKV) infection and vice versa, and consequently, increase disease severity (3-5). While an Ebola vaccine has shown promise recently (6), it is not yet approved. Moreover, there is no effective antiviral treatment available against DENV, EBOV, ZIKV and most other emerging viral pathogens, leaving the global population at risk for significant morbidity and mortality.

Most antiviral therapies approved to date target viral enzymes (e.g., protease or polymerase) via a “one drug, one bug” approach. This approach has demonstrated measurable success in treating chronic viral infections, such as hepatitis C virus (HCV). However, such an approach to drug development is inefficient, expensive and, therefore, not easily scalable to address the large unmet clinical need (7). Moreover, targeting virally-encoded factors by monotherapy often is associated with rapid emergence of drug resistance (7). One alternative approach to treating viral infections while increasing the barrier to resistance is to target host functions, which the viruses intimately rely on (7). Moreover, focusing on host factors commonly required by multiple viral pathogens could provide broad-spectrum coverage. The host-targeted approach is attractive, particularly for the treatment of emerging viral infections lacking any treatment, given the

opportunities to repurpose already existing drugs that are known to modulate specific host functions with tolerable side effect and toxicity profiles.

Intracellular membrane traffic is one of many cellular processes hijacked by viruses. Membrane traffic relies, in part, on the interactions between adaptor protein complexes (AP1 through AP-5) and the transmembrane cargo. The well characterized clathrin-associated APs, AP1 and AP2, are heterotetrameric complexes, which orchestrate the formation of vesicles destined for bidirectional transport in the secretory pathway and for endocytosis from the plasma membrane, respectively (8). The two host cell kinases, AP2-associated protein kinase 1 (AAK1) and cyclin G-associated kinase (GAK) regulate receptor mediated endocytosis and *trans*-Golgi network (TGN) transport (9-12). Specifically, AAK1 and GAK phosphorylate the  $\mu$  subunits of AP1 and AP2, thereby enhancing their binding affinity for sorting motifs within the cargo (9, 10, 13-15). Moreover, GAK recruits clathrin-associated APs to the plasma membrane and TGN (16).

Other groups have implicated APs in the lifecycle of multiple unrelated viruses (17-26), and we reported roles for AP2 in HCV entry and assembly (22, 23). Our work demonstrated that through AP2 phosphorylation, AAK1 and GAK regulate these temporally distinct steps of the HCV lifecycle, thereby, for the first time, uncovering their role as “master regulators” of a viral infection (22, 23). Moreover, we reported that sunitinib and erlotinib, approved anticancer drugs with potent binding to AAK1 and GAK (dissociation constant ( $K_d$ ) of 11 and 3.1 nM, respectively (27)), or selective, chemically distinct GAK inhibitors, block HCV entry and assembly in tissue culture (22, 23, 28). Although clathrin APs are presumed to mediate intracellular viral trafficking, this hypothesis has not been addressed in live cells. Moreover, the

114 roles of AAK1 and GAK in viral infections beyond HCV and their in vivo functional relevance  
115 remain unknown. In the present study, we demonstrate a role for AAK1- and GAK-regulated  
116 AP1 activity in HCV release and document that HCV particles specifically co-traffic with AP1  
117 and AP2 in live cells. We also show a requirement for AAK1 and GAK in the lifecycles of  
118 DENV and EBOV. Furthermore, we provide support for the feasibility of repurposing  
119 sunitinib/erlotinib combination as a broad-spectrum antiviral approach using in vitro models of  
120 multiple viral infections and murine models of DENV and EBOV. Lastly, we characterize the  
121 mechanism of action of sunitinib and erlotinib by validating AAK1 and GAK as critical  
122 mediators of the antiviral effect and revealing additional potential antiviral host targets, which  
123 include AXL Receptor Tyrosine Kinase, KIT Proto-Oncogene Receptor Tyrosine Kinase, and  
124 RET Proto-Oncogene.

## Results

### APs co-traffic with HCV and orchestrate infection

To determine the differential roles of AP1 and AP2 in HCV infection, we examined the effect of depleting their  $\mu$  subunits in Huh7.5 human hepatoma cells on distinct steps of the viral lifecycle. Successful depletion of each targeted AP was confirmed (**Figure 1A**), with no alteration in the expression of the non-targeted AP (data not shown). AP2 depletion reduced HCV entry, had no effect on HCV RNA replication, and reduced HCV assembly (i.e.; reduced intra- and extracellular infectivity in lysates and culture supernatants derived from HCV transfected cells, respectively), as we previously reported (**Figure 1, B-D**) (22, 23). In contrast, AP1 depletion reduced extracellular infectivity only (**Figure 1, B-D**), consistent with a defect in viral release, in agreement with prior reports (29, 30). To test whether in addition to AP2 (22), phosphorylation of AP1 by AAK1 and GAK is important for infectious HCV production, we studied the effect of overexpressing phosphorylation site mutant AP1 (T144A) on HCV infectivity (**Figure 1E**) (31). Intracellular infectivity was not affected by overexpression of either wild type or T144A AP1 (**Figure 1F**). In contrast, extracellular infectivity increased upon ectopic expression of wild type AP1 and decreased with ectopic expression of T144A AP1 (**Figure 1F**). Thus, viral release emerges as yet another step of the HCV lifecycle, beyond entry and assembly, which is regulated by AAK1 and GAK.

While APs were postulated to directly mediate intracellular viral trafficking, this has never been addressed experimentally in live cells with any virus. To test the hypothesis that HCV particles shuttle with clathrin APs intracellularly, we utilized live cell imaging. The co-trafficking of individual, infectious HCV particles harboring a tetracysteine (TC) tag within the core protein

(TC-core) with AP1- or AP2-mCherry was monitored (32). We previously have shown that TC-core motility requires HCV virion assembly (32). Analysis of TC-core puncta stained with the biarsenical dye FIAH revealed that a large fraction of motile TC-core co-trafficked with either AP1 (25%) or AP2 (38%), whereas only 3% co-trafficked with the autophagosomal marker LC3 (**Figure 1, G and H, Supplemental Figure 1A and Supplemental Movie 1-3**). The velocities of the co-trafficking particles were consistent with previous reports on secretory vesicle trafficking as well as TC-core puncta co-trafficking with vesicle-associated membrane protein (VAMP) (32, 33) (**Supplemental Figure 1B**). AP2-associated TC-core puncta motility was reduced significantly upon mutation (Y136A) of a Yxx $\Phi$  motif within core, a motif critical for AP2 binding and HCV assembly (22), as measured by the overall distance traveled (**Figure 1I and Supplemental Movie 4**). These findings provide direct experimental evidence for a role of clathrin-associated APs in mediating intracellular virus trafficking. Specifically, these imaging data combined with our current and previous characterization of the roles of AP1 and AP2 in the lifecycle of HCV (22, 23), support the hypothesis that AP1 co-traffics with HCV during viral release, while AP2 co-traffics with HCV during viral entry and subsequently to the sites of assembly.

To understand whether drug modulation of adaptor protein phosphorylation by AAK1 and GAK manifests itself in an intracellular trafficking defect, we studied the effect of sunitinib and erlotinib, approved drugs with potent anti-AAK1 and/or GAK activity, on HCV particle trafficking by live cell imaging. Treatment of HCV-infected cells with sunitinib and erlotinib reduced motility of TC-core puncta co-trafficking with AP1 and AP2 (**Figure 1J and**



**Supplemental Movies 5-10**). These findings support our hypothesis that the antiviral effect of sunitinib and erlotinib is associated with reduced intracellular viral traffic.

### **The role of AAK1 and GAK in DENV infection in cells**

The requirement for AAK1 and GAK in viral infections beyond HCV is unknown. To investigate whether another, distantly related member of the *Flaviviridae* family relies on these regulatory kinases and their associated AP targets, we examined the effect of the corresponding gene silencing on DENV infection in human hepatoma (Huh7) cells. We observed a requirement for AP2, but not AP1 in DENV entry using cell lines stably expressing short hairpin RNA (shRNA) targeting AP1, AP2 or a non-targeting (NT) sequence (**Figure 2, A and B**). While depletion of AP1 and AP2 had no effect on DENV RNA replication as measured by subgenomic replicon assays (34) (**Figure 2C**), it diminished the production of infectious virus in culture supernatants (**Figure 2D**). Silencing expression of AAK1 and GAK resulted in no apparent cytotoxic effect (**Figure 2, E and F**), but analogous to experiments with HCV inhibited entry and infectious virus production of DENV, with no effect on RNA replication (**Figure 2, G-I**). These results implicate AAK1 and GAK in the DENV lifecycle via regulation of two temporally distinct steps that depend on the clathrin-associated APs; entry and infectious virus production.

To determine whether a comparable effect on DENV infection can be achieved pharmacologically and further validate AAK1 and GAK as antiviral targets, we treated DENV-infected cells with selective AAK1 and GAK inhibitors. 7737 and 7745 are imidazo[1,2-b]pyridazine-based compounds originally developed to modulate AAK1 activity as a potential treatment of neurological disorders ( $K_d = 1$  nM,  $IC_{50} < 10$  nM) (**Figure 2J and Supplemental**

**Figure 2**) (35). Isothiazolo[5,4-b]pyridines, 12g and 12i (**Figure 2K**), are potent ( $K_d = \sim 8$  nM), selective, ATP-competitive GAK inhibitors capable of restricting HCV infection (28). We measured a dose-dependent inhibition of the DENV2 infection following a 2-day drug treatment with all four compounds, with EC<sub>50</sub>s of 1.5-5.1  $\mu$ M (**Figure 2, J and K**). The concentration range yielding at least 1 log reduction in viral infection showed minimal or no toxicity as measured by alamarBlue® assays.

Together, these results validate AAK1 and GAK as regulators of DENV infection and point to their pharmacological inhibition as a potential anti-DENV strategy.

### **Sunitinib and erlotinib have a synergistic anti-DENV effect and a high genetic barrier to resistance in vitro**

To determine whether a similar effect on DENV infection can be achieved with approved drugs with potent anti-AAK1 and/or GAK activity, we treated DENV-infected cells with sunitinib and erlotinib (**Figure 3A**). Consistent with published HCV data (22, 23), we measured a dose-dependent inhibition of DENV2 infection following a 2-day drug treatment with an EC<sub>50</sub> of 0.51  $\mu$ M for sunitinib and 6.5  $\mu$ M for erlotinib by luciferase assays (**Figure 3, B and C**). The concentration range yielding at least 2 log reduction in viral infection showed minimal or no toxicity as measured by alamarBlue® assays with CC<sub>50</sub>s of 8.0  $\mu$ M for sunitinib and >50  $\mu$ M for erlotinib (**Figure 3, B and C and Table 1**). Similar results were demonstrated by standard plaque assays (**Supplemental Figure 3A**). Notably, treatment with combinations of the two drugs revealed synergistic inhibition of DENV2 infection with a synergy volume of 36.7  $\mu$ M<sup>2</sup>% at the 95% confidence interval and no synergistic toxicity (**Figure 3, D and E and**

**Supplemental Figure 3B**). Importantly, sunitinib and erlotinib also dose-dependently inhibited infection of DENV1, DENV3 and DENV4 (**Table 1**).

To determine if DENV can escape treatment with sunitinib and erlotinib, we passaged DENV in the presence of sunitinib/erlotinib combination or the DENV non-structural (NS) 4B protein inhibitor, SDM25N, at increasing concentrations (0.5-2.5  $\mu$ M) corresponding to values between EC50 and EC90. Infectious virus output was quantified over several passages by plaque assays. By passage 8, DENV4 overcame inhibition by SDM25N with the emergence of a previously characterized resistance mutation in NS4B (P101L, analogous to P104L in DENV2) (36). In contrast, DENV4 was cleared from the culture by passage 6 under the sunitinib/erlotinib treatment without any phenotypic resistance (**Figure 3F**). These results point to sunitinib/erlotinib combination as a potential anti-DENV strategy with a higher relative barrier to resistance than a direct-acting antiviral.

#### **Broad-spectrum activity of sunitinib and erlotinib**

Next, we studied the effect of sunitinib and erlotinib on replication of two additional flaviviruses, West Nile virus (WNV) and ZIKV. Sunitinib dose-dependently inhibited both WNV and ZIKV by focus-formation and plaque assays with EC50 of 0.51-0.55  $\mu$ M, whereas erlotinib demonstrated some efficacy only against ZIKV with EC50 of 6.28  $\mu$ M (**Supplemental Figure 4, A and B and Table 1**).

We also investigated whether EBOV, a member of an unrelated viral family (*Filoviridae*), whose entry depends on AP1 and AP2 activity (18, 37-39), may be similarly dependent on AAK1 and

GAK. To test this hypothesis, we silenced AAK1 and GAK expression in Vero cells (**Figure 4A**) and measured infection of vesicular stomatitis virus encapsidated RNA (encoding a GFP reporter gene) pseudotyped with EBOV glycoproteins (rVSV-GP EBOV). Quantification of GFP positive cells at the 20 hour time point by flow cytometry revealed that AAK1 and GAK depletion reduced infection relative to NT control (**Figure 4C**) without impacting cell viability (**Figure 4B**). A similar level of inhibition was observed upon quantification of viral RNA at 3 hours post-infection, highlighting a defect in the entry step (**Supplemental Figure 5A**). These data further validate AAK1 and GAK as targets for broad-spectrum antiviral therapy. Moreover, treatment of Vero cells with sunitinib and erlotinib resulted in a dose-dependent decrease in rVSV-GP EBOV infection measured by flow cytometry 20 hours post-infection and entry measured by qRT-PCR 3 hours post-infection (Figure 4D and **Supplemental Figure 5B**). Although, the effect of erlotinib measured by flow cytometry was modest relative to that of sunitinib, combination treatment displayed measurable synergy in inhibiting entry with a synergy volume of 147.05  $\mu\text{M}^2\%$  at the 95% confidence interval and zero synergistic toxicity (**Figure 4, E and F**). Next, we tested the ability of these drugs to inhibit authentic EBOV infection in Huh7 cells. Sunitinib treatment resulted in a dose-dependent reduction in EBOV infection with EC50 value of 0.47  $\mu\text{M}$  and CC50 greater than 10  $\mu\text{M}$ , whereas erlotinib showed moderate activity with EC50 of 12.9  $\mu\text{M}$  and no appreciable cytotoxicity at the concentrations tested (**Figure 4H and Table 1**).

To explore more broadly the spectrum of coverage provided by sunitinib and erlotinib, we studied their antiviral effects against additional unrelated viruses. Viral infection was measured in various cell lines following three day treatment regimens. We detected antiviral activity of either or both drugs against RNA viruses in six families (**Table 1**), including *Togaviridae* (e.g.,

chikungunya virus), *Arenaviridae* (e.g., Junin virus), and *Paramyxoviridae* (e.g., respiratory syncytial virus). These data expand the possible indications of sunitinib and/or erlotinib as antiviral agents beyond *Flaviviridae* infections, to other established and emerging RNA viruses.

#### **Sunitinib/erlotinib combinations are effective in vivo**

To address the therapeutic potential of sunitinib and erlotinib as antiviral agents, we tested their application in a murine model of dengue. We measured viral burden and mortality in an alpha/beta and gamma interferon receptor-deficient murine model of dengue on 129/Sv (AG-129) (40, 41) and C57BL/6 (AG-B6) genetic backgrounds. In a prophylaxis model, we initiated once daily treatment of AG-B6 mice with 30-60 mg/kg of sunitinib and erlotinib in combination or individually concurrently with DENV inoculation and analyzed viremia at 48 hours. The doses tested for each drug were at or near the equivalent of approved human dose as calculated based on the body surface area per FDA's guidelines (42). These doses were below the maximum tolerated dose (MTD) in mice and confirmed to be non-toxic in our dengue model (42-44). Treatment with erlotinib did not alter viremia, whereas sunitinib alone marginally reduced it (**Figure 5A**). Consistent with our in vitro synergy results, daily administration of the combination treatment resulted in 11-fold reduction in viral RNA (**Figure 5A**). In addition, we measured a significant reduction of the infectious virus load by plaque assays in the serum as well as spleen and liver in mice treated with 30 mg/kg doses of sunitinib and erlotinib relative to vehicle controls (**Supplemental Figure 6A**). Pharmacokinetic analysis revealed that within the first 6 hours of administration each drug concentration in the serum, as measured by liquid chromatography-tandem mass spectrometry (LC-MS/MS), exceeded the corresponding EC50 concentration deduced from our in vitro data (**Supplemental Figure 6B**). Moreover, the synergy

between sunitinib and erlotinib predicts even more potency in combination. Although sunitinib and erlotinib were largely cleared from the serum by 18 hours, which is in contrast with the slower clearance rates reported in humans (44, 45), both drugs concentrate several fold within tissues where DENV replicates, such as liver (46, 47). To maintain higher serum drug concentration, we next administered 30 mg/kg drug combination at 12 hour intervals and measured viremia. The twice daily drug administration resulted in an even more apparent reduction of viral load relative to vehicle control (**Figure 5B**). Notably, drug administration reduced viral load from day 2 to 3 post-infection in contrast to an increase in viral load within the control arm during that time.

To assess whether the reduction in viral load would translate into improved disease outcome, we determined the effect of combination treatment with sunitinib and erlotinib on morbidity and mortality in AG-129 and AG-B6 mice. Following infection with a lethal DENV inoculum, we initiated once daily drug administration at a dose sufficient to significantly reduce viremia (i.e. 30 mg/kg of each drug). The animals were monitored twice daily and euthanized when moribund (48). The experiment was concluded when all the remaining animals regained full mobility and displayed weight gain for at least two consecutive days. Upon a 5-day drug treatment regimen given either intraperitoneally or orally, we observed a significant reduction in morbidity and mortality of infected animals relative to vehicle controls (**Figure 5, C and D**). Specifically, 100% of vehicle-treated mice succumbed to infection on day 4-8 post-infection, whereas sunitinib/erlotinib treatment protected 75-100% of the mice. This combination treatment proved efficacious with either intraperitoneal or oral administration, the latter of which is approved for use in humans (**Figure 5, C and D**). We also compared the effect of daily treatment with the

individual drugs to that of the combination. In this trial, 94% of vehicle-treated AG-129 mice succumbed to infection; treatment with erlotinib did not alter survival, whereas sunitinib alone offered partial (37%) protection. Consistent with our in vitro synergy results, we observed the greatest protection (62%) from mortality with combination drug treatment (**Figure 5E**). Furthermore, even when the combination drug treatment was initiated at various time points after infection the mice remained protected relative to vehicle control, albeit mice treated at 48 hours after inoculation eventually succumbed to infection (**Figure 5F**).

Given the observed potency of sunitinib and sunitinib/erlotinib combination against EBOV infection in vitro, we assessed in vivo efficacy of these drugs in a murine model of Ebola. Drugs were administered daily intraperitoneally for 10 days beginning at 6 hours prior to infection. As with the dengue model, the chosen doses were at or near the equivalent of approved human dose, below the MTD in mice, and confirmed to be non-toxic in our Ebola model. All mice demonstrated signs of morbidity as evident by weight loss during the first 7-10 days post-infection (**Figure 5G**). 90% of vehicle-treated mice succumbed to infection on days 6-13 post-infection; treatment with erlotinib at 45 mg/kg did not alter animal survival, whereas 5 mg/kg sunitinib alone increased survival to 30% (**Figure 5H**). Consistent with our in vitro synergy results, we observed greatest weight gain and survival (50%) with a combination drug treatment.

Together, these results demonstrate therapeutic potential of sunitinib/erlotinib combinations against infections with two unrelated emerging RNA viruses.

**Mechanisms underlying the antiviral effects of sunitinib and erlotinib in vitro and in vivo.**

To better understand the target(s) and mechanism of action underlying the anti-DENV activity of sunitinib and erlotinib, we first probed the steps of the viral lifecycle affected by these compounds. We detected interference precisely with the steps inhibited via siRNAs against AAK1 and GAK (**Figure 2, G and I**), namely entry and infectious DENV production (**Figure 6, A-C**). Notably, DENV RNA replication, a step commonly inhibited by direct-acting antivirals (7), was not affected by these drugs. This phenotype supports a hypothesis that inhibition of AAK1 and GAK likely contributes to the anti-DENV effect of these drugs.

To confirm that the antiviral activity is correlated with functional inhibition of AAK1 and GAK activity, we measured levels of phospho-AP2 upon drug treatment. Dose-dependent reduction in the phospho-AP2 to total AP2 ratio was demonstrated in DENV-infected cells (**Figure 6D**). Next, we conducted gain of function assays to further validate AP2, a substrate for both AAK1 and GAK, as a key mediator of the anti-DENV effect of these drugs. Ectopic expression of wild type but not T156A phosphorylation AP2 mutant or vector control either partially or completely rescued the antiviral effect of sunitinib/erlotinib combination (**Figure 6, E and F**). These results indicate that AAK1- and GAK-mediated phosphorylation of AP2 is a mechanism underlying the antiviral effect of sunitinib and erlotinib against DENV.

Next, we determined whether these drugs exert their antiviral effect in vivo by similarly inhibiting phosphorylation of the AAK1 and GAK ligand, AP2. Liver tissue lysates harvested from AG-B6 mice 3 hours post drug administration revealed dose-dependent inhibition of AP2 phosphorylation upon treatment with sunitinib and erlotinib, and most markedly with the



combination (**Figure 6G**). These results provide evidence that drug exposure in animals is associated with modulation of AP2.

These data combined with the finding that more selective AAK1 and GAK inhibitors lacking affinity to most of sunitinib's and erlotinib's cancer targets (e.g. VEGFR and EGFR) (28, 35) have anti-DENV activity, indicate that AAK1 and GAK are important mediators of the observed antiviral effect. Nevertheless, these data cannot rule out additional potential cellular targets mediating the anti-DENV activity of these compounds. Whereas erlotinib's target selectivity is quite narrowly focused on EGFR and GAK with significantly less affinity for other kinases, sunitinib is a multi-target kinase inhibitor (49, 50). We thus examined the effects of siRNA-mediated depletion of 27 major kinases targeted by these small molecules ( $K_d < 20$  nM) on DENV infection and cellular viability. Using a cut-off of greater than 50% inhibition of viral infection as measured by luciferase assays normalized to cell viability in two independent screens, we identified AXL Receptor Tyrosine Kinase, KIT Proto-Oncogene Receptor Tyrosine Kinase, and RET Proto-Oncogene as possible antiviral targets of our kinase inhibitors in addition to AAK1 and GAK (**Figure 6H**). However, silencing of KIT also substantially reduced cellular viability (**Supplemental Figure 7**).

Taken together, our data indicate that inhibition of AP-mediated intracellular membrane trafficking regulated by AAK-1 and GAK represents an important mechanism by which sunitinib and erlotinib inhibit DENV infection in vitro and in vivo and that additional mechanisms, potentially mediated by other kinases, may act in concert.

## Discussion

Clathrin-associated AP1 and AP2 complexes have been implicated in orchestrating multiple viral infections, however, their precise mechanistic involvement was not characterized. Moreover, the relevance of AAK1 and GAK, kinase regulators of these APs that we discovered as essential for HCV infection, to other viral infections remained unknown. Here, we addressed this knowledge gap and evaluated the therapeutic potential of inhibiting AAK1 and GAK as a broad-spectrum antiviral strategy. Integrating RNAi, dominant interfering, pharmacological and molecular virology approaches we demonstrate roles for AP1 and AP2 complexes as well as AAK1 and GAK in entry and assembly/release of *Flaviviridae* family members and validate these host factors as attractive targets for broad-spectrum antiviral therapy (**Figure 7**). We establish that sunitinib and erlotinib inhibit DENV and EBOV infections in vitro and in vivo, and are potent in vitro against WNV, ZIKV and RNA viruses from four additional families, including *Togaviridae*, *Arenaviridae*, *Paramyxoviridae* and *Retroviridae*. Together, our data illustrate the utility of these two clinically approved compounds both as tools to identify host factors important in viral infection as well as potential therapies against emerging viral infections.

Using advanced live cell imaging, we provide the first direct evidence that viral particles co-traffic intracellularly with AP complexes. Our imaging findings exclude a theory whereby AP complexes contribute to viral infections solely by recruiting or mediating intracellular traffic of host cargo components essential for the viral lifecycle.

We show that sunitinib and erlotinib, potent, albeit non-selective inhibitors of AAK1 and GAK, respectively, restrict DENV and EBOV infections in vitro and their combination reduces

viremia, morbidity, and mortality in the relevant murine models. Replication assays demonstrating efficacy against viral species in six unrelated families (Table 1) further support our broad-spectrum hypothesis, though in vivo efficacy beyond dengue and Ebola remains to be tested. AAK1 and GAK have partially overlapping functions (12, 23), which may explain moderate antiviral effect in vitro with either sunitinib or erlotinib, yet synergistic activity upon treatment with both. The synergy also may result from inhibition of additional targets by these compounds. Although the observed reduction in DENV load was relatively modest in mice, it correlated with a significant survival benefit, comparable to the report on host alpha-glucosidase inhibitor, Celgosivir (51), which yielded 100% protection from mortality with less than tenfold reduction in viremia. Importantly, the sunitinib/erlotinib combination remained protective in the mouse model of dengue even when administered after established infection, thereby supporting its promise as both prophylaxis and therapy.

We provide multiple lines of evidence to support modulation of AAK1 and GAK activity as an important mode of antiviral action of sunitinib and erlotinib in the dengue model. We demonstrate that these drugs inhibit both DENV entry and infectious virus production, analogous to the phenotype seen with RNAi-mediated suppression of clathrin-associated APs and AAK1 and GAK. Additionally, we demonstrate antiviral effects of more selective AAK1 and GAK inhibitors. Due to lack of affinity to most sunitinib's and erlotinib's cancer targets (e.g. VEGFR and EGFR) (28, 35), the activity of the selective compounds further confirms that AAK1 and GAK are relevant antiviral targets. While the more selective GAK inhibitors also bind KIT, more work is required to validate whether KIT is an anti-DENV target. Furthermore, we characterized the mechanism by which the pharmacological inhibition of AAK1 and GAK mediates the anti-

dengue effect. We establish that antiviral activity of sunitinib and erlotinib correlates with reduced phospho-AP2 levels in vitro. In accordance with this observation, we show that wild type but not a phosphorylation AP2 mutant can rescue the anti-dengue effect of these drugs. We provide evidence that this mechanism also plays a role in vivo by demonstrating that antiviral activity correlates with reduced AP2 phosphorylation in tissues upon drug treatment. These findings reveal that a block in AP2 phosphorylation mechanistically explains at least in part the antiviral effect of AAK1 and GAK inhibitors. These findings also present AP2 phosphorylation as a useful pharmacodynamic biomarker in potential future clinical studies. We further demonstrate that sunitinib and erlotinib reduce HCV-AP1 and AP2 co-trafficking by live cell imaging, thereby validating this mode of action at the molecular level. While AP-mediated intracellular membrane trafficking likely represents a primary mechanism by which AAK1 and GAK regulate viral infection, additional substrates of these kinases, such as NUMB, also may contribute to this function (23).

We explore the possible involvement of additional targets with  $K_d$ 's of 20 nM or less reported for sunitinib and erlotinib using an siRNA library against 27 kinases. Our siRNA screen reveals that none of the other major targets of erlotinib beyond GAK, namely EGFR and STK10, affect DENV infection. In contrast, at least three additional targets of sunitinib, beyond AAK1, namely AXL, KIT and RET, may facilitate DENV infection and thus, potentially also mediate sunitinib's antiviral effect. AXL is an already known attachment factor/signaling receptor for multiple RNA viruses, including DENV, EBOV and possibly ZIKV (52-55). Although confirmatory studies with AXL-deficient cells are required, inhibition of AXL by sunitinib may contribute to its effect on DENV entry. KIT and RET are paralogs with no reported roles in RNA viral infections and

await further investigation. Given our inability to silence expression of KIT without a substantial negative impact on cell viability (likely due to its role in cell survival and proliferation (56)), its specific relevance to DENV infection remains unclear. Overall, our data underscore the utility of using sunitinib and erlotinib as pharmacological probes to identify novel host factors required for viral infection.

We speculate that inhibition of AAK1 and GAK accounts for these drugs' effect against a broad-spectrum of viruses, particularly those previously shown to depend on AP1 and AP2 activity, such as EBOV (18, 37-39). Inhibition of additional kinases including AXL, KIT and RET may play a role. Though most of the EC50 values we report fall in the low micromolar range for the 6 viral families tested (Table 1), the relative potency of sunitinib and erlotinib varies between the different viral species. Such differences can be attributed to both variations in the assays employed and the likely distinct dependence on the various host factors targeted by these inhibitors in the lifecycle of different viruses. Other mechanisms of action, such as modulation of immune responses also could contribute to the protective phenotype observed in vivo.

Although toxicity is a concern when targeting host functions, finding a safe therapeutic window may be feasible. Sunitinib and erlotinib each are approved as a once daily oral treatment for multiple cancers at doses comparable to those exhibiting antiviral activity in vivo. A combination therapy already has been evaluated clinically and was tolerated, albeit with an increase in the adverse events primarily related to gastrointestinal disturbances (57, 58). However, a shift from the long-term treatment of cancer to acute infection such as with DENV should improve tolerance and minimize adverse effects. The safety and efficacy of sunitinib and/or erlotinib will

be evaluated in dengue patients in the near future and potentially in patients with EBOV disease in future outbreaks (ClinicalTrials.gov NCT02380625).

The vast genetic diversity of viral species and replication strategies challenges the design of broadly effective direct-acting antivirals, however, a host-targeted approach could circumvent this issue. Sunitinib and erlotinib inhibit all four DENV serotypes. Moreover, a broad-spectrum therapy, such as with sunitinib/erlotinib combination could be used to treat DENV-CHIKV (59, 60) or DENV-ZIKV (61) co-infections and infections with newly emerging RNA viruses. It also can be administered even prior to an accurate diagnosis of a viral threat, thereby increasing protection. Furthermore, although viral resistant mutations can emerge during treatment with host-targeted approaches (62), targeting host proteins that are not under the genetic control of viruses is more likely to have a higher barrier to resistance than classical direct-acting antivirals. This is exemplified by our data and treatment with cyclophilin inhibitors (63). We recognize, however, that our dengue resistance assay is somewhat limited by the short-term virus passage. Although we predict that the genetic barrier to resistance is high, it may be possible to select for resistance over longer-term passage under different conditions or in a different, chronic infection model. Lastly, viruses utilize similar strategies to cancer cells for overcoming drug-mediated inhibition. Simultaneous inhibition of several kinases or targeting several pathways by the same drug or drug combination may prove attractive in combating viral pathogens, as previously shown in cancer (64). Such “polypharmacology” by a single drug could increase the effectiveness while minimizing viral resistance.

In summary, our study serves as a proof-of-concept for the feasibility of identifying novel host-targeted broad-spectrum antiviral therapies via both repurposing and development of novel chemical entities. Such approaches may provide additive and possibly synergistic effects in combination with other strategies being developed to combat emerging viral infections.

## Methods

**Plasmids and virus constructs.** ORFs encoding AP1M1 (AP1) and AP2M1 (AP2) were selected from the Human ORFeome library of cDNA clones (65) (Open Biosystems) and recombined into either pCherry (for mCherry fluorescence protein tagging) or pGLuc (for Gaussia Princeps luciferase fragment (Gluc) tagging) vectors using Gateway technology (Invitrogen). GFP-LC3 construct was previously described (66). pFLJ6/JFH(p7-Rluc2A) was a gift from Charles M. Rice (67). HCV TC-core was previously described (32). Plasmids used in the HCVpp entry assays (pNL4-3.Luc.R-E, pcDM8, and pcDM8-E1E2) were a gift from Shoshana Levy. DENV2 TSV01 Renilla reporter plasmid was a gift from Pei-Yong Shi (68). Lentiviral constructs used for AP2 overexpression were cloned into the pRRLSIN backbone. rVSV-GP-EBOV construct was a gift from Kartik Chandran (69). Mouse adapted N124D/K128E DENV2 PL046 was a gift from Sujana Shrestha (70). pCMV-DV2Rep was a gift from Andrew Yueh (34). Mutations were introduced by site-directed mutagenesis using the QuikChange kit (Stratagene).

**Cells.** Huh7 (Apath LLC), Huh7.5 (Apath LLC), BHK-21 (ATCC), and Vero (ATCC) cells were grown in DMEM (Mediatech) supplemented with 10% FBS, nonessential amino acids (Gibco), 1% L-glutamine (Gibco), and 1% penicillin-streptomycin (Gibco) and maintained in a humidified incubator with 5% CO<sub>2</sub> at 37°C. C6/36 cells were grown in Leibovitz's L-15 media (CellGro) supplemented with 10% FBS and 1% HEPES in a humidified chamber at 28°C and 0% CO<sub>2</sub>.



**Reagents.** The following reagents were used: sunitinib malate (Selleckchem), erlotinib (LC Laboratories), Captisol (Captisol), siImporter (Millipore), Lipofectamine2000 (Invitrogen). 12 g and 12i were synthesized by the Herdewijn laboratory (28). 7737 and 7745 were synthesized by ACME Bioscience, Inc.

**Western Blotting and Antibodies.** Cells were lysed in M-Per protein extraction reagent (ThermoFisher). For phosphor-protein detection, cells were pre-treated with 100 nM calyculin A (Cell Signaling), PP1 and PP2a phosphatase inhibitor, for 30 minutes prior to lysis. Liver tissue was homogenized in RIPA buffer supplemented with Halt protease and phosphatase inhibitor cocktail (ThermoFisher) and 100 nM calyculin A using 0.9-2 mm stainless steel beads in a BBX24 Bullet Blender homogenizer (NextAdvance). Clarified protein lysates were run on 4-12% Bis-Tris gels (Invitrogen), transferred onto PVDF membranes (BioRad). Blots were blocked and blotted with anti-AP1M1 (Abcam, Cat. #ab111135), anti-AP2M1 (Abcam, Cat. #ab75995), anti-GLuc (New England BioLabs, Cat. #E8023S), anti-phospho-AP2M1 (T156) (Cell Signaling, Cat. #3843S), anti-AAK1 (Abcam, Cat. #ab134971), anti-GAK (MBL International, Cat. #MO573), anti-beta actin (Sigma-Aldrich, Cat. #A3854) antibodies. Signal was detected with peroxidase (HRP)-conjugated secondary antibodies. Band intensity was quantified with ImageJ software.

**RNA interference (RNAi).** siRNAs (100 to 250 nM) were transfected into cells using siIMPORTER (Millipore) 48 hours prior to infection. Sequences/catalog numbers are as follows: human AAK1 and GAK, Silencer Select pre-designed siRNA ID#s22494 and s5529, respectively (ThermoFisher); Chlorocebus sabaeus (green monkey) AAK1 siRNA#1,

GGUAUAUGUUGGAACCAGATT, AAK1 siRNA#2, GAAUAUUGUGGGUUACAUUTT,  
GAK siRNA#1, GCAUUAAGAGGCUAUUAUTT, GAKsiRNA #2,  
CAGCAUCCAUAGGAAAAGATT. NT, Silencer Select negative control. Infections were  
performed at 48 hours post-transfection. AP1M1 and AP2M1 were silenced via transduction  
with shRNA-expressing lentivirus (TRCN0000218336, TRCN0000060239 or Mission pLKO.1-  
puro non-mammalian shRNA control; Sigma-aldrich) and selection on 1 µg/ml puromycin.  
Custom Cherry-Pick ON-TARGETplus siRNA library against 27 kinase genes was purchased  
from Dharmacon (see **Supplemental Table 1** for gene and siRNA sequence details).

**Virus Production.** HCV 2a J6/JFH(p7-Rluc2A) was transcribed in vitro using Megascript T7 kit  
(Ambion) and DENV2 TSV01 (used for DENV in vitro assays) or N124D/K128E DENV2  
PL046 (used for DENV in vivo infections) RNA were transcribed in vitro using  
mMessage/mMachine (Ambion) kits. HCVcc and HCVpp were produced as previously  
described (23). DENV was produced by electroporating RNA into BHK-21 cells, harvesting  
supernatants at day 10 and titering via standard plaque assays on BHK-21 cells. In parallel, on  
day 2 post-electroporation DENV-containing supernatant was used to inoculate C6/36 cells to  
amplify the virus For in vivo experiments, DENV supernatant was concentrated 100-fold by  
centrifugation at 50,000 x g. rVSV-GP EBOV was propagated and titered on Vero cells via  
fluorescent-focus assay(69).

**Entry Assays.** Huh7.5 cells were infected with HCVpp (71) and 8 µg/ml Polybrene for 4 hours.  
Firefly luciferase activity was measured at 48-72 hours post-infection. DENV2 entry was  
measured at 6 hours post-infection of Huh7 cells by monitoring *Renilla* luciferase activity.

Luminescence was detected on InfiniteM1000 plate reader (Tecan). Vero cells were infected with rVSV-GP EBOV for 3 hours, total RNA harvested, reverse-transcribed and EBOV GP transcript normalized to GAPDH quantified by real-time PCR.

**Infection Assays.** Huh7 cells were infected with DENV or ZIKV in replicates (n=3-10) for 4 hours at MOI of 0.01. Overall infection was measured at 48 hours using either a *Renilla* luciferase substrate or by plaque assays. Vero cells were infected with rVSV-GP EBOV for 4 hours and washed. At 20 hours post-infection cells were fixed with 4% formaldehyde and analyzed on LSR II cytometer (BD Biosciences) using FITC channel. Data were processed using FlowJo software. EBOV infection was carried out under BSL-4 conditions. 48 hours after infection, cells were formalin-fixed and infection was measured by immunofluorescence using KZ52 anti-EBOV antibody in an Operetta HCS using the Harmony software package. Other viral infection assays, conducted by the Diamond lab (WNV), IBT Bioservices (CHIKV, RSV, JUNV) and NIH/NIAID (others) were performed as summarized in **Table 1**.

**RNA Replication Assays.** HCV RNA replication was measured 72 hours post-electroporation, as previously described (22). DENV2 replication assays were performed as previously described (34). Briefly, Huh7 cells were transfected with DNA-launched DENV2 replicon, pCMV-DV2Rep along with TET-ON plasmids. 36 hours post-transfection viral RNA transcription was induced by doxycycline and shut down by changing to doxycycline-free medium 6 hours later. Replication was monitored by luciferase activity every day for three days. Data were normalized to activity at 24 hours post-induction.

**Infectious virus production.** Infectious HCV or DENV production (i.e. extracellular infectivity) was measured in culture supernatants of cells electroporated with viral RNA for 48-72 hours and used to infect naïve cells for 48 hours. Intracellular HCV infectivity was measured by inoculating naïve cells with lysates of electroporated cells subjected to 4 rounds of free-thawing and clarified at 5,000 x g, as described (22).

**Pharmacological inhibition.** For entry assays, cells were pre-treated with the inhibitors or DMSO for 1 hour prior to and for the duration of the infection, followed by replacement with drug-free medium. For the overall infection, RNA replication or infectious virus production assays, inhibitors were left in for the duration of the study.

**Gain of function assays.** WT or T156A AP2 or empty vector control was expressed ectopically in Huh7 cells by lentiviral transduction. 24 hours post-transduction cells were pre-treated with sunitinib and erlotinib, infected with luciferase reporter DENV at MOI of 0.01 and incubated for 72 hours prior to luciferase and viability assays.

**Live cell imaging.** Huh7.5 cells were infected with concentrated HCV TC-core (32) at MOI of 1 for 24 hours, then transfected with either AP1- or AP2-mCherry using Lipofectamine2000 (Invitrogen) and seeded onto collagen-coated 35 mm fluorodishes (World Precision Instruments). At 72 hours post-infection, cells were labeled with biarsenical dye (1.25  $\mu$ M) in Opti-MEM at 37°C for 30 minutes, then washed three times with 1X BAL (2,3-dimercapto-1-propanol) wash buffer (Invitrogen) supplemented with 500  $\mu$ M EDT in Opti-MEM. The cells were washed and incubated in prewarmed imaging media (DMEM-F12, Invitrogen)

supplemented with 10% fetal bovine serum, 0.1 mM nonessential amino acids, 1% penicillin-streptomycin, and 25 mM HEPES. When specified, TC-core infected cells were incubated with DMSO, sunitinib (4 $\mu$ M) or erlotinib (10 $\mu$ M) beginning at 24 hours post-infection. Timelapse images were taken using a Leica SP5 II AOBS Tandem Scanner Spectral confocal microscope with a 100X 1.46 oil objective and a heated (37°C) chamber. An average of 5 movies representing individual cells with trackable 15-30 puncta each were recorded per sample with sequential frames taken every 2 seconds. Individual core puncta run lengths and transport velocities were calculated using the Manual Tracking plugin for Image J, measuring the distance traveled (in any direction) between frames for a respective TC-core puncta.

**Resistance studies.** DENV4 (BC287/97) was used to inoculate Huh7 cells at MOI of 0.01 and passaged every 3 days by transferring an equal volume of viral supernatant to naïve cells under increasing drug selection (0.5-1.5 $\mu$ M, passage 1-6; 2.5  $\mu$ M passage 7, 8). Upon completion of 8 passages, virus from the resulting supernatants was titered by plaque assays. SDM25N resistance mutation in NS4B at passage 8 was confirmed by purifying and reverse transcribing viral RNA from supernatants of cells treated with DMSO or SDM25N as described in the RNA extraction and quantification section. NS4B region was amplified with iProof<sup>TM</sup> high-fidelity PCR kit (Bio-Rad) using primers NS4B Fwd-GATGTGGAYYTGAGACCAGCYTCAGCATGGAC and NS4B Rev-AGTCAANACTTCACAGAAAGCCCATGTTGTTCTCATCAA (N=any base, Y=C or T) and sequenced (Sequetech Corporation).

**In vivo dengue studies.** AG129 mice deficient in type I and II IFN receptors were obtained from Dr. Harry Greenberg. Mice were backcrossed to C57B6/6J for N=10 generations to obtain

congenic AG-B6 strain. Age-matched, male and female mice at 8 to 10 weeks of age were used for all experiments. Mouse adapted N124D/K128E DENV2 ( $5 \times 10^5$  pfu produced in BHK-21 cells or  $10^7$  pfu produced in C6/36 cells) was inoculated retroorbitally into mice under general and local anesthesia. Drugs were administered at the indicated doses in a total volume of 100-200  $\mu$ l per animal using 10% Captisol as vehicle. Drugs or vehicle were administered intraperitoneally or orally once or twice daily starting at the time of inoculation or at various time points post-inoculation for a total of 3-5 days. Mice were monitored twice daily until the conclusion of the experiment. Moribund animals were euthanized by carbon dioxide inhalation. Serum was isolated from whole blood harvested retroorbitally at 48 or 72 hours post DENV inoculation under general and local anesthesia. Tissues were harvested following euthanasia and snap frozen on dry ice until further analysis.

#### **In vivo Ebola studies**

Groups of 10 female C57BL/6 mice (8-12 weeks of age) purchased from Jackson Laboratories (Bar Harbor, Maine) were treated with drugs or vehicle 6 hours prior to viral challenge. Erlotinib and sunitinib were administered intraperitoneally at the indicated doses in a total volume of 200  $\mu$ l using 10% Captisol as vehicle. A group of 10 mice was left untreated to allow for interpretation of any survival seen in the vehicle treated group. Mice were inoculated intraperitoneally with 100 pfu of mouse-adapted EBOV. Mice were then treated once daily for a total of 10 days and observed daily for 28 days for lethality or clinical signs of disease.

**Animal study approval/Ethics Statement.** Animal research was conducted under a protocol approved by Stanford's Institutional Animal Care and Use Committee (Administrative Panel on

Laboratory Animal Care) and its Institutional Biosafety Committee (Administrative Panel on Biosafety) or by the US Army Medical Research Institute of Infectious Diseases (USAMRIID) Institutional Animal Care and Use Committee (IACUC) in compliance with the Animal Welfare Act and other federal statutes and regulations relating to animals and experiments involving animals. The Stanford and USAMRIID animal facilities are AAALAC-accredited and adhere to the principles stated in the Guide for the Care and Use of Laboratory Animals. DENV and EBOV challenge studies were conducted in BSL2 and maximum containment BSL4 facility, respectively. Moribund mice were humanely euthanized on the basis of IACUC-approved criteria.

**RNA extraction and quantification.** Total RNA from cells was isolated using RNA purification kit (Macherey-Nagel). Mouse serum was purified from whole blood using Terumo Capiject Capillary Blood collection tubes (ThermoFisher). Tissues were homogenized using 0.9-2 mm stainless steel beads in a BBX24 Bullet Blender homogenizer (NextAdvance). Total RNA from serum and tissues was extracted with QIAamp UltraSens Virus kit (Qiagen). cDNA was generated using high-capacity cDNA reverse transcription kit (Invitrogen). DENV RNA was quantified by qRT-PCR using TaqMan GEX master mix (ThermoFisher), AAK1, GAK, EBOV GP and housekeeping gene (GAPDH) RNA were quantified using iTaq Universal SYBR Green Supermix (BioRad) on a StepOnePlus real-time PCR system (Applied Biosystems). Primers and probes sequences are as follows: DENV2 Fwd (GAGAGCAGATCTCTGATGAATAA), DENV2 Rev (ACTGTTGCACAGTCGACAC), DENV2 Probe (TATGCTGAAACGCGAGAGAAACCGC), GAPDH Fwd (GAAATCCCATCACCATCTTCCAG), GAPDH Rev (GAGCCCCAGCCTTCTCCATG).

**Viability assays.** Viability was assessed using AlamarBlue® reagent (Invitrogen) according to manufacturer's protocol. Fluorescence was detected at 560 nm on InfiniteM1000 plate reader (Tecan).

**Data analysis of combination drug treatment.** Synergy/antagonism analysis was performed using the MacSynergy II program as described (23, 72). Matrix data sets in four replicates were assessed at the 95% confidence level for each experiment. Synergy and log volume were calculated. As suggested by Prichard et al. (72), such data sets should be interpreted as follows: volumes of synergy or antagonism at values of  $<25 \mu\text{M}^2\%$  are insignificant, those of 25 to  $50 \mu\text{M}^2\%$  are minor but significant, those of 50 to  $100 \mu\text{M}^2\%$  are moderate and probably important in vivo, and those of  $>100 \mu\text{M}^2\%$  are strong and likely to be important in vivo.

**Statistical analysis.** All data were analyzed with GraphPad Prism software. Fifty percent effective concentrations ( $\text{EC}_{50}$ ) were measured by fitting data to a three-parameter logistic curve. *P* values were calculated by two-tailed unpaired *t*-test or two-way ANOVA with Bonferroni post test for in vitro data sets and by Mann-Whitney test for in vivo data sets. Survival curve *p* values were calculated by log-ranked Mantel-Cox test.



**Author contributions**

Conceived and designed the experiments: SE, EB, GN, AS, SP, JB, RBB, JG, MSD, JD, GR.

Performed the experiments: EB, GN, AS, SP, JB, SW, FX, RBB, JG, CN. Analyzed the data: SE,

EB, GN, AS, SP, JB, SW, FX, RBB, JG, MSD, JD, GR. Contributed reagents/materials/models:

RM, CN, SDJ, PH. Wrote the paper: EB, SE. SE supervised the overall project.

**Acknowledgments:** This work was supported by award number 1U19AI10966201 (CETR) from the National Institute of Allergy and Infectious Diseases (NIAID) to S.E, NIAID U19 AI083019 to M.S.D, grant RSG-14-11 0-0 1-MPC from the American cancer society to S.E and G.R., and grants from Stanford Bio-X, the Stanford SPARK program, and the Stanford Translational Research and Applied Medicine (TRAM) program. In vitro studies were also supported by grant 2013100 from the Doris Duke Charitable Foundation. G.N. was supported by the Child Health Research Institute, Lucile Packard Foundation for Children's Health, as well as the Stanford CSTA (grant number UL1 TR000093). S.P. was supported by Taiwan Ministry of Science and Technology grant 103-2917-I-564-033. Dr. Dye's work kindly acknowledges the support of JSTO-DTRA (CB3958) in completion of the live virus experiments. The opinions, interpretations, conclusions, and recommendations are those of the authors and are not necessarily endorsed by the U.S. Army or the other funders.

We thank Scott Weaver and Robert Tesh for the ZIKV (MR766), Mark N. Prichard for providing the MacSynergy II program, Kartik Chandran for the rVSV-GP EBOV construct, and Eva Harris and Karla Kirkegaard for assistance with establishing dengue tissue culture and mouse models in our laboratory.

## References

1. Bhatt, S., Gething, P.W., Brady, O.J., Messina, J.P., Farlow, A.W., Moyes, C.L., Drake, J.M., Brownstein, J.S., Hoen, A.G., Sankoh, O., et al. 2013. The global distribution and burden of dengue. *Nature* 496:504-507.
2. Flipse, J., and Smit, J.M. 2015. The Complexity of a Dengue Vaccine: A Review of the Human Antibody Response. *PLoS Negl Trop Dis* 9:e0003749.
3. Priyamvada, L., Quicke, K.M., Hudson, W.H., Onlamoon, N., Sewatanon, J., Edupuganti, S., Pattanapanyasat, K., Chokephaibulkit, K., Mulligan, M.J., Wilson, P.C., et al. 2016. Human antibody responses after dengue virus infection are highly cross-reactive to Zika virus. *Proc Natl Acad Sci U S A*.
4. Dejnirattisai, W., Supasa, P., Wongwiwat, W., Rouvinski, A., Barba-Spaeth, G., Duangchinda, T., Sakuntabhai, A., Cao-Lormeau, V.M., Malasit, P., Rey, F.A., et al. 2016. Dengue virus sero-cross-reactivity drives antibody-dependent enhancement of infection with Zika virus. *Nat Immunol*.
5. Stettler, K., Beltramello, M., Espinosa, D.A., Graham, V., Cassotta, A., Bianchi, S., Vanzetta, F., Minola, A., Jaconi, S., Mele, F., et al. 2016. Specificity, cross-reactivity and function of antibodies elicited by Zika virus infection. *Science*.
6. Henao-Restrepo, A.M., Longini, I.M., Egger, M., Dean, N.E., Edmunds, W.J., Camacho, A., Carroll, M.W., Doumbia, M., Draguez, B., Duraffour, S., et al. 2015. Efficacy and effectiveness of an rVSV-vectored vaccine expressing Ebola surface glycoprotein: interim results from the Guinea ring vaccination cluster-randomised trial. *Lancet* 386:857-866.
7. Bekerman, E., and Einav, S. 2015. Infectious disease. Combating emerging viral threats. *Science* 348:282-283.
8. Park, S.Y., and Guo, X. 2014. Adaptor protein complexes and intracellular transport. *Biosci Rep* 34.
9. Olusanya, O., Andrews, P.D., Swedlow, J.R., and Smythe, E. 2001. Phosphorylation of threonine 156 of the mu2 subunit of the AP2 complex is essential for endocytosis in vitro and in vivo. *Curr Biol* 11:896-900.
10. Ricotta, D., Conner, S.D., Schmid, S.L., von Figura, K., and Honing, S. 2002. Phosphorylation of the AP2 mu subunit by AAK1 mediates high affinity binding to membrane protein sorting signals. *J Cell Biol* 156:791-795.
11. Umeda, A., Meyerholz, A., and Ungewickell, E. 2000. Identification of the universal cofactor (auxilin 2) in clathrin coat dissociation. *Eur J Cell Biol* 79:336-342.
12. Zhang, C.X., Engqvist-Goldstein, A.E., Carreno, S., Owen, D.J., Smythe, E., and Drubin, D.G. 2005. Multiple roles for cyclin G-associated kinase in clathrin-mediated sorting events. *Traffic* 6:1103-1113.
13. Ghosh, P., and Kornfeld, S. 2003. AP1 binding to sorting signals and release from clathrin-coated vesicles is regulated by phosphorylation. *J Cell Biol* 160:699-708.
14. Conner, S.D., and Schmid, S.L. 2002. Identification of an adaptor-associated kinase, AAK1, as a regulator of clathrin-mediated endocytosis. *J Cell Biol* 156:921-929.
15. Fingerhut, A., von Figura, K., and Honing, S. 2001. Binding of AP2 to sorting signals is modulated by AP2 phosphorylation. *J Biol Chem* 276:5476-5482.

16. Lee, D.W., Zhao, X., Zhang, F., Eisenberg, E., and Greene, L.E. 2005. Depletion of GAK/auxilin 2 inhibits receptor-mediated endocytosis and recruitment of both clathrin and clathrin adaptors. *J Cell Sci* 118:4311-4321.
17. Alconada, A., Bauer, U., and Hoflack, B. 1996. A tyrosine-based motif and a casein kinase II phosphorylation site regulate the intracellular trafficking of the varicella-zoster virus glycoprotein I, a protein localized in the trans-Golgi network. *EMBO J* 15:6096-6110.
18. Bhattacharyya, S., Hope, T.J., and Young, J.A. 2011. Differential requirements for clathrin endocytic pathway components in cellular entry by Ebola and Marburg glycoprotein pseudovirions. *Virology* 419:1-9.
19. Dutta, D., Chakraborty, S., Bandyopadhyay, C., Valiya Veetil, M., Ansari, M.A., Singh, V.V., and Chandran, B. 2013. EphrinA2 regulates clathrin mediated KSHV endocytosis in fibroblast cells by coordinating integrin-associated signaling and c-Cbl directed polyubiquitination. *PLoS Pathog* 9:e1003510.
20. Huang, H.C., Chen, C.C., Chang, W.C., Tao, M.H., and Huang, C. 2012. Entry of hepatitis B virus into immortalized human primary hepatocytes by clathrin-dependent endocytosis. *J Virol* 86:9443-9453.
21. Humphries, A.C., Dodding, M.P., Barry, D.J., Collinson, L.M., Durkin, C.H., and Way, M. 2012. Clathrin potentiates vaccinia-induced actin polymerization to facilitate viral spread. *Cell Host Microbe* 12:346-359.
22. Neveu, G., Barouch-Bentov, R., Ziv-Av, A., Gerber, D., Jacob, Y., and Einav, S. 2012. Identification and targeting of an interaction between a tyrosine motif within hepatitis C virus core protein and AP2M1 essential for viral assembly. *PLoS Pathog* 8:e1002845.
23. Neveu, G., Ziv-Av, A., Barouch-Bentov, R., Berkerman, E., Mulholland, J., and Einav, S. 2015. AP2-associated protein kinase 1 and cyclin G-associated kinase regulate hepatitis C virus entry and are potential drug targets. *J Virol* 89:4387-4404.
24. Ohka, S., Ohno, H., Tohyama, K., and Nomoto, A. 2001. Basolateral sorting of human poliovirus receptor alpha involves an interaction with the mu1B subunit of the clathrin adaptor complex in polarized epithelial cells. *Biochem Biophys Res Commun* 287:941-948.
25. Ohno, H., Aguilar, R.C., Fournier, M.C., Hennecke, S., Cosson, P., and Bonifacino, J.S. 1997. Interaction of endocytic signals from the HIV-1 envelope glycoprotein complex with members of the adaptor medium chain family. *Virology* 238:305-315.
26. Agrawal, T., Schu, P., and Medigeshi, G.R. 2013. Adaptor protein complexes-1 and 3 are involved at distinct stages of flavivirus life-cycle. *Sci Rep* 3:1813.
27. Karaman, M.W., Herrgard, S., Treiber, D.K., Gallant, P., Atteridge, C.E., Campbell, B.T., Chan, K.W., Ciceri, P., Davis, M.I., Edeen, P.T., et al. 2008. A quantitative analysis of kinase inhibitor selectivity. *Nat Biotechnol* 26:127-132.
28. Kovackova, S., Chang, L., Berkerman, E., Neveu, G., Barouch-Bentov, R., Chaikuad, A., Heroven, C., Sala, M., De Jonghe, S., Knapp, S., et al. 2015. Selective Inhibitors of Cyclin G Associated Kinase (GAK) as Anti-Hepatitis C Agents. *J Med Chem* 58:3393-3410.
29. Benedicto, I., Gondar, V., Molina-Jimenez, F., Garcia-Buey, L., Lopez-Cabrera, M., Gastaminza, P., and Majano, P.L. 2015. Clathrin mediates infectious hepatitis C virus particle egress. *J Virol* 89:4180-4190.

- 870 30. Coller, K., Heaton, N., Berger, K., Cooper, J., Saunders, J., and Randall, G. 2012.  
871 Molecular determinants and dynamics of hepatitis C virus secretion. *PLoS Pathog*  
872 8:e1002466-e1002466.
- 873 31. Sorensen, E.B., and Conner, S.D. 2008. AAK1 regulates Numb function at an early step  
874 in clathrin-mediated endocytosis. *Traffic* 9:1791-1800.
- 875 32. Coller, K.E., Heaton, N.S., Berger, K.L., Cooper, J.D., Saunders, J.L., and Randall, G.  
876 2012. Molecular determinants and dynamics of hepatitis C virus secretion. *PLoS Pathog*  
877 8:e1002466.
- 878 33. Wacker, I., Kaether, C., Kromer, A., Migala, A., Almers, W., and Gerdes, H.H. 1997.  
879 Microtubule-dependent transport of secretory vesicles visualized in real time with a GFP-  
880 tagged secretory protein. *J Cell Sci* 110 ( Pt 13):1453-1463.
- 881 34. Yang, C.C., Tsai, M.H., Hu, H.S., Pu, S.Y., Wu, R.H., Wu, S.H., Lin, H.M., Song, J.S.,  
882 Chao, Y.S., and Yueh, A. 2013. Characterization of an efficient dengue virus replicon for  
883 development of assays of discovery of small molecules against dengue virus. *Antiviral*  
884 *Res* 98:228-241.
- 885 35. Bi, Y., Carson, K.G., Cianchetta, G., Green, M.A., KUMI, G., LIANG, Z., LIU, Y.J.,  
886 Main, A., Zhang, Y., and ZIPP, G.G. Imidazo [1, 2-b] pyridazine-based compounds,  
887 compositions comprising them, and uses thereof. US Patent publication number  
888 WO2013134219 A1 filed 5 Mar. 2013.
- 889 36. van Cleef, K.W., Overheul, G.J., Thomassen, M.C., Kaptein, S.J., Davidson, A.D.,  
890 Jacobs, M., Neyts, J., van Kuppeveld, F.J., and van Rij, R.P. 2013. Identification of a new  
891 dengue virus inhibitor that targets the viral NS4B protein and restricts genomic RNA  
892 replication. *Antiviral Res* 99:165-171.
- 893 37. Bhattacharyya, S., Mulherkar, N., and Chandran, K. 2012. Endocytic pathways involved  
894 in filovirus entry: advances, implications and future directions. *Viruses* 4:3647-3664.
- 895 38. Poirier, S., Mayer, G., Murphy, S.R., Garver, W.S., Chang, T.Y., Schu, P., and Seidah,  
896 N.G. 2013. The cytosolic adaptor AP1A is essential for the trafficking and function of  
897 Niemann-Pick type C proteins. *Traffic* 14:458-469.
- 898 39. Carette, J.E., Raaben, M., Wong, A.C., Herbert, A.S., Obernosterer, G., Mulherkar, N.,  
899 Kuehne, A.I., Kranzusch, P.J., Griffin, A.M., Ruthel, G., et al. 2011. Ebola virus entry  
900 requires the cholesterol transporter Niemann-Pick C1. *Nature* 477:340-343.
- 901 40. Johnson, A.J., and Roehrig, J.T. 1999. New mouse model for dengue virus vaccine  
902 testing. *J Virol* 73:783-786.
- 903 41. Schul, W., Liu, W., Xu, H.Y., Flamand, M., and Vasudevan, S.G. 2007. A dengue fever  
904 viremia model in mice shows reduction in viral replication and suppression of the  
905 inflammatory response after treatment with antiviral drugs. *J Infect Dis* 195:665-674.
- 906 42. Nair, A.B., and Jacob, S. 2016. A simple practice guide for dose conversion between  
907 animals and human. *J Basic Clin Pharm* 7:27-31.
- 908 43. Mendel, D.B., Laird, A.D., Xin, X., Louie, S.G., Christensen, J.G., Li, G., Schreck, R.E.,  
909 Abrams, T.J., Ngai, T.J., Lee, L.B., et al. 2003. In vivo antitumor activity of SU11248, a  
910 novel tyrosine kinase inhibitor targeting vascular endothelial growth factor and platelet-  
911 derived growth factor receptors: determination of a pharmacokinetic/pharmacodynamic  
912 relationship. *Clin Cancer Res* 9:327-337.
- 913 44. Higgins, B., Kolinsky, K., Smith, M., Beck, G., Rashed, M., Adames, V., Linn, M.,  
914 Wheeldon, E., Gand, L., Birnboeck, H., et al. 2004. Antitumor activity of erlotinib (OSI-

- 774, Tarceva) alone or in combination in human non-small cell lung cancer tumor xenograft models. *Anticancer Drugs* 15:503-512.
45. Haznedar, J.O., Patyna, S., Bello, C.L., Peng, G.W., Speed, W., Yu, X., Zhang, Q., Sukbuntherng, J., Sweeny, D.J., Antonian, L., et al. 2009. Single- and multiple-dose disposition kinetics of sunitinib malate, a multitargeted receptor tyrosine kinase inhibitor: comparative plasma kinetics in non-clinical species. *Cancer Chemother Pharmacol* 64:691-706.
46. Chee, E.L., Lim, A.Y., Modamio, P., Fernandez-Lastra, C., and Segarra, I. 2016. Sunitinib tissue distribution changes after coadministration with ketoconazole in mice. *Eur J Drug Metab Pharmacokinet* 41:309-319.
47. Zerbe, L.K., Dwyer-Nield, L.D., Fritz, J.M., Redente, E.F., Shroyer, R.J., Conklin, E., Kane, S., Tucker, C., Eckhardt, S.G., Gustafson, D.L., et al. 2008. Inhibition by erlotinib of primary lung adenocarcinoma at an early stage in male mice. *Cancer Chemother Pharmacol* 62:605-620.
48. Orozco, S., Schmid, M.A., Parameswaran, P., Lachica, R., Henn, M.R., Beatty, R., and Harris, E. 2012. Characterization of a model of lethal dengue virus 2 infection in C57BL/6 mice deficient in the alpha/beta interferon receptor. *J Gen Virol* 93:2152-2157.
49. 2008. SuperNova Life Science, Human Kinome Heat Map, <http://www.supernovalifescience.com/HM/HM%2041.pdf>.
50. Davis, M.I., Hunt, J.P., Herrgard, S., Cicceri, P., Wodicka, L.M., Pallares, G., Hocker, M., Treiber, D.K., and Zarrinkar, P.P. 2011. Comprehensive analysis of kinase inhibitor selectivity. *Nat Biotechnol* 29:1046-1051.
51. Rathore, A.P., Paradkar, P.N., Watanabe, S., Tan, K.H., Sung, C., Connolly, J.E., Low, J., Ooi, E.E., and Vasudevan, S.G. 2011. Celgosivir treatment misfolds dengue virus NS1 protein, induces cellular pro-survival genes and protects against lethal challenge mouse model. *Antiviral Res* 92:453-460.
52. Brindley, M.A., Hunt, C.L., Kondratowicz, A.S., Bowman, J., Sinn, P.L., McCray, P.B., Jr., Quinn, K., Weller, M.L., Chiorini, J.A., and Maury, W. 2011. Tyrosine kinase receptor Axl enhances entry of Zaire ebolavirus without direct interactions with the viral glycoprotein. *Virology* 415:83-94.
53. Meertens, L., Carnec, X., Lecoin, M.P., Ramdasi, R., Guivel-Benhassine, F., Lew, E., Lemke, G., Schwartz, O., and Amara, A. 2012. The TIM and TAM families of phosphatidylserine receptors mediate dengue virus entry. *Cell Host Microbe* 12:544-557.
54. Hamel, R., Dejarnac, O., Wichit, S., Ekchariyawat, P., Neyret, A., Luplertlop, N., Perera-Lecoin, M., Surasombatpattana, P., Talignani, L., Thomas, F., et al. 2015. Biology of Zika Virus Infection in Human Skin Cells. *J Virol* 89:8880-8896.
55. Nowakowski, T.J., Pollen, A.A., Di Lullo, E., Sandoval-Espinosa, C., Bershteyn, M., and Kriegstein, A.R. 2016. Expression Analysis Highlights AXL as a Candidate Zika Virus Entry Receptor in Neural Stem Cells. *Cell Stem Cell* 18:591-596.
56. Roskoski, R., Jr. 2005. Signaling by Kit protein-tyrosine kinase--the stem cell factor receptor. *Biochem Biophys Res Commun* 337:1-13.
57. Scagliotti, G.V., Krzakowski, M., Szczesna, A., Strausz, J., Makhson, A., Reck, M., Wierzbiicki, R.F., Albert, I., Thomas, M., Miziara, J.E., et al. 2012. Sunitinib plus erlotinib versus placebo plus erlotinib in patients with previously treated advanced non-small-cell lung cancer: a phase III trial. *J Clin Oncol* 30:2070-2078.

58. Blumenschein, G.R., Jr., Ciuleanu, T., Robert, F., Groen, H.J., Usari, T., Ruiz-Garcia, A., Tye, L., Chao, R.C., and Juhasz, E. 2012. Sunitinib plus erlotinib for the treatment of advanced/metastatic non-small-cell lung cancer: a lead-in study. *J Thorac Oncol* 7:1406-1416.
59. Chipwaza, B., Mugasa, J.P., Selemani, M., Amuri, M., Mosha, F., Ngatunga, S.D., and Gwakisa, P.S. 2014. Dengue and Chikungunya Fever among Viral Diseases in Outpatient Febrile Children in Kilosa District Hospital, Tanzania. *PLoS Negl Trop Dis* 8:e3335.
60. Karthik, R., Vineetha, K. R., Raut, C. G., Nazim Shaik and Manjunatha. 2014. Seroprevalance of dengue and chikungunya co infection and its clinical correlation in bangalore city hospitals. *International Journal of Current Research* 6:11040-11044.
61. Dupont-Rouzeyrol, M., O'Connor, O., Calvez, E., Daures, M., John, M., Grangeon, J.P., and Gourinat, A.C. 2015. Co-infection with Zika and dengue viruses in 2 patients, New Caledonia, 2014. *Emerg Infect Dis* 21:381-382.
62. de Wispelaere, M., LaCroix, A.J., and Yang, P.L. 2013. The Small Molecules AZD0530 and Dasatinib Inhibit Dengue Virus RNA Replication via Fyn Kinase. *Journal of Virology* 87:7367-7381.
63. Lin, K., and Gallay, P. 2013. Curing a viral infection by targeting the host: the example of cyclophilin inhibitors. *Antiviral Res* 99:68-77.
64. Knight, Z.A., Lin, H., and Shokat, K.M. 2010. Targeting the cancer kinome through polypharmacology. *Nat Rev Cancer* 10:130-137.
65. Rual, J.F., Hirozane-Kishikawa, T., Hao, T., Bertin, N., Li, S., Dricot, A., Li, N., Rosenberg, J., Lamesch, P., Vidalain, P.O., et al. 2004. Human ORFeome version 1.1: a platform for reverse proteomics. *Genome Res* 14:2128-2135.
66. Heaton, N.S., and Randall, G. 2010. Dengue virus-induced autophagy regulates lipid metabolism. *Cell Host Microbe* 8:422-432.
67. Tscherne, D.M., Jones, C.T., Evans, M.J., Lindenbach, B.D., McKeating, J.A., and Rice, C.M. 2006. Time- and temperature-dependent activation of hepatitis C virus for low-pH-triggered entry. *J Virol* 80:1734-1741.
68. Zou, G., Xu, H.Y., Qing, M., Wang, Q.Y., and Shi, P.Y. 2011. Development and characterization of a stable luciferase dengue virus for high-throughput screening. *Antiviral Res* 91:11-19.
69. Chandran, K., Sullivan, N.J., Felbor, U., Whelan, S.P., and Cunningham, J.M. 2005. Endosomal proteolysis of the Ebola virus glycoprotein is necessary for infection. *Science* 308:1643-1645.
70. Prestwood, T.R., Prigozhin, D.M., Sharar, K.L., Zellweger, R.M., and Shresta, S. 2008. A mouse-passaged dengue virus strain with reduced affinity for heparan sulfate causes severe disease in mice by establishing increased systemic viral loads. *J Virol* 82:8411-8421.
71. Bartosch, B., Dubuisson, J., and Cosset, F.L. 2003. Infectious hepatitis C virus pseudo-particles containing functional E1-E2 envelope protein complexes. *J Exp Med* 197:633-642.
72. Prichard, M.N., and Shipman, C., Jr. 1996. Analysis of combinations of antiviral drugs and design of effective multidrug therapies. *Antivir Ther* 1:9-20.

## Figure Legends

**Figure 1. AP1 and AP2 co-traffic with HCV and orchestrate infection.** (A) Confirmation of gene expression knockdown by Western blot in Huh7.5 cells stably expressing AP shRNA or non-targeting control (NT). (B) Entry of HCV pseudoparticles (HCVpp) was measured by luciferase assays at 48 hours post-infection. (C) HCV RNA replication measured via luciferase assays 72 hours post HCV RNA electroporation. (D) HCV infectivity measured via luciferase assays by inoculating naïve cells with lysates (intracellular) and supernatants (extracellular) from electroporated cells. (E) AP1 ectopic expression following transfection of Huh7.5 cells with GLuc-tagged WT, T144A AP1, or an empty control; blotted with anti-GLuc antibody. (F) HCV intra- and extracellular infectivity in AP1 overexpressing cells vs. control. Shown are mean  $\pm$  s.d. (n=3-10). (G) Representative live cell fluorescence microscopy montages of TC-core HCV (green) co-trafficking with AP1- and AP2-mCherry (red). Distance traveled ( $\mu$ m) and time elapsed (min:s) during video acquisition are indicated. (H) Quantification of motile TC-core puncta co-trafficking with AP1, AP2 and LC3. (I) Quantification of distance traveled per acquisition of WT or Y136A mutant TC-Core HCV associated with AP2. (J) Quantification of distance traveled per acquisition of TC-Core HCV associated with AP1 or AP2 upon treatment with sunitinib (4  $\mu$ M) and erlotinib (10  $\mu$ M). Results in panels B-D and F represent data pooled from at least two independent experiments each with 6-10 biological replicates. Panels H-J are representative experiments out of at least three conducted. Shown are mean  $\pm$  s.d.; \*\*\*p<0.001 relative to corresponding NT (B-D), empty vector control (F), WT TC-core (I) or vehicle control (J) (two-tailed unpaired t-test).

**Figure 2. AP1, AP2 and their regulatory kinases, AAK1 and GAK, are essential for DENV infection in vitro.** (A) Confirmation of stable shRNA- or (E) transient siRNA-mediated gene expression silencing by Western blot in Huh7 cells. (B and G) DENV entry measured via luciferase assay 6 hours post-infection. (C, H) DENV RNA replication monitored by luciferase activity every 24 hours following transfection of Huh7 cells with a Tet-inducible DNA-launched DENV replicon and induction by doxycycline for 6 hours (GND is a replication incompetent DENV). Data are normalized to signal at 24 hours. (D, I) Infectious DENV production measured via luciferase assays by inoculating naïve cells with supernatants from stable or siRNA-transfected cells 48 hours post-electroporation with DENV RNA. (F) Relative cell viability following gene expression knockdown measured by alamarBlue assays. (J and K) Cell viability (blue) and dose response of DENV infection (black) to more selective AAK1 (J) and GAK (K) inhibitors (structures shown) measured by luciferase assays 48 hours post-infection. Data are plotted relative to vehicle control. Shown are representative experiments from at least two conducted. Individual experiments in panels B-D and F-K had 8-10 biological replicates, shown are mean  $\pm$  s.d.; \*\*\*p<0.001 relative to corresponding NT control (two-tailed unpaired t-test). (N.s., non-significant).

**Figure 3. Sunitinib and erlotinib have a synergistic anti-DENV effect and a high genetic barrier to resistance in vitro.** (A) Chemical structures of the indicated drugs. (B and C) Cellular viability (blue) and dose response of overall DENV infection (black) to sunitinib and erlotinib measured by luciferase assays at 48 hours post-infection. Data are plotted relative to vehicle control. (D and E) Synergy/antagonism at the 95% confidence interval (CI) of



sunitinib/erlotinib combination treatment on antiviral effect (D) and cellular viability (E) computed by MacSynergy II. (F) DENV4 was used to infect Huh7 cells and passaged every 72 hours by inoculating naïve cells with equal volumes of viral supernatants under DMSO treatment or selection with sunitinib and erlotinib (SM+E) or SDM25N (DENV NS4B inhibitor) increasing from 0.5 to 2.5  $\mu$ M over 8 passages. Viral titers were measured by plaque assays at every other passage (PFU, plaque forming units). Dashed line represents assay detection limit. Results in panels B and C represent data pooled from at least two independent experiments. Data in panels D-F are representative of at least two experiments. Shown in panels B, C, and F are mean  $\pm$  s.d. Individual experiments in panels B-E and F had 5-10 and 2 biological replicates, respectively.

**Figure 4. Inhibition of AAK1 and GAK suppresses EBOV infection.** (A) Confirmation of siRNA-mediated gene expression silencing by qPCR in Vero cells. Shown is normalized gene expression relative to GAPDH at 48 hours post-transfection. (B) Relative cell viability measured by alamarBlue assays and (C) rVSV-GP EBOV infection of Vero cells measured by flow cytometry at 20 hours post-infection of AAK1- and GAK-depleted cells. \*\*\* $p$ <0.001 relative to NT (two-tailed unpaired t-test). (D) Dose response of rVSV-GP EBOV infection to 4 hour treatment with inhibitors measured by flow cytometry at 20 hours post-infection in Vero cells. (E and F) Synergy/antagonism of sunitinib/erlotinib combination treatment on rVSV-GP EBOV infection (E) and cell viability (F). (H) Dose response to drug treatment in Huh7 cells under BSL-4 containment following 48 hour with EBOV infection (black) measured by immunostaining with an anti-GP antibody and cell viability (blue) measured by Hoescht counterstain and quantified by high content imager. Data are plotted relative to vehicle control. All data shown are representative of at least two experiments; panels B-H have 3 biological replicates each. Shown in panels B-D and H are mean  $\pm$  s.d.

**Figure 5. AAK1 and GAK inhibitors are protective in murine models of dengue and Ebola.** (A) DENV viremia in AG-B6 mice measured by qRT-PCR on day 2 post-infection following once daily administration of vehicle, sunitinib (SM) and/or erlotinib (E). (B) DENV viremia in AG-B6 mice on days 2 and 3 post-infection following twice daily drug administration. (C) Weight loss and (D) mortality of DENV-infected AG-B6 mice treated once daily for 5 days with vehicle or sunitinib/erlotinib combination ( $n$ =8 per treatment group). (E) Mortality of DENV-infected AG-129 mice treated once daily for 5 days with vehicle, sunitinib and/or erlotinib (data are pooled from two independent experiments,  $n$ =8-16 per treatment group). (F) Mortality of DENV-infected AG-B6 mice treated once daily with vehicle or sunitinib/erlotinib combination beginning at the indicated hour post-inoculation, T0-T48 (data are pooled from two independent experiments,  $n$ =8-16 per treatment group). (G) Weight loss and (H) mortality of EBOV-infected C57/B6 mice treated once daily for 10 days with vehicle, sunitinib and/or erlotinib ( $n$ =10 per treatment group). Doses are in mg/kg. Administration was IP, except when denoted PO (C and D), at inoculation (A-E, G, and H) or post-inoculation (F). Panels A-D and G-H are representative of two or more independent experiments. \* $p$ <0.05; \*\* $p$ <0.01; \*\*\* $p$ <0.001 relative to vehicle control (Mann-Whitney test). Survival analysis (D-F and H) was done with log-rank (Mantel-Cox) test;  $p$  values are relative to vehicle control. (GE, genomic equivalents).

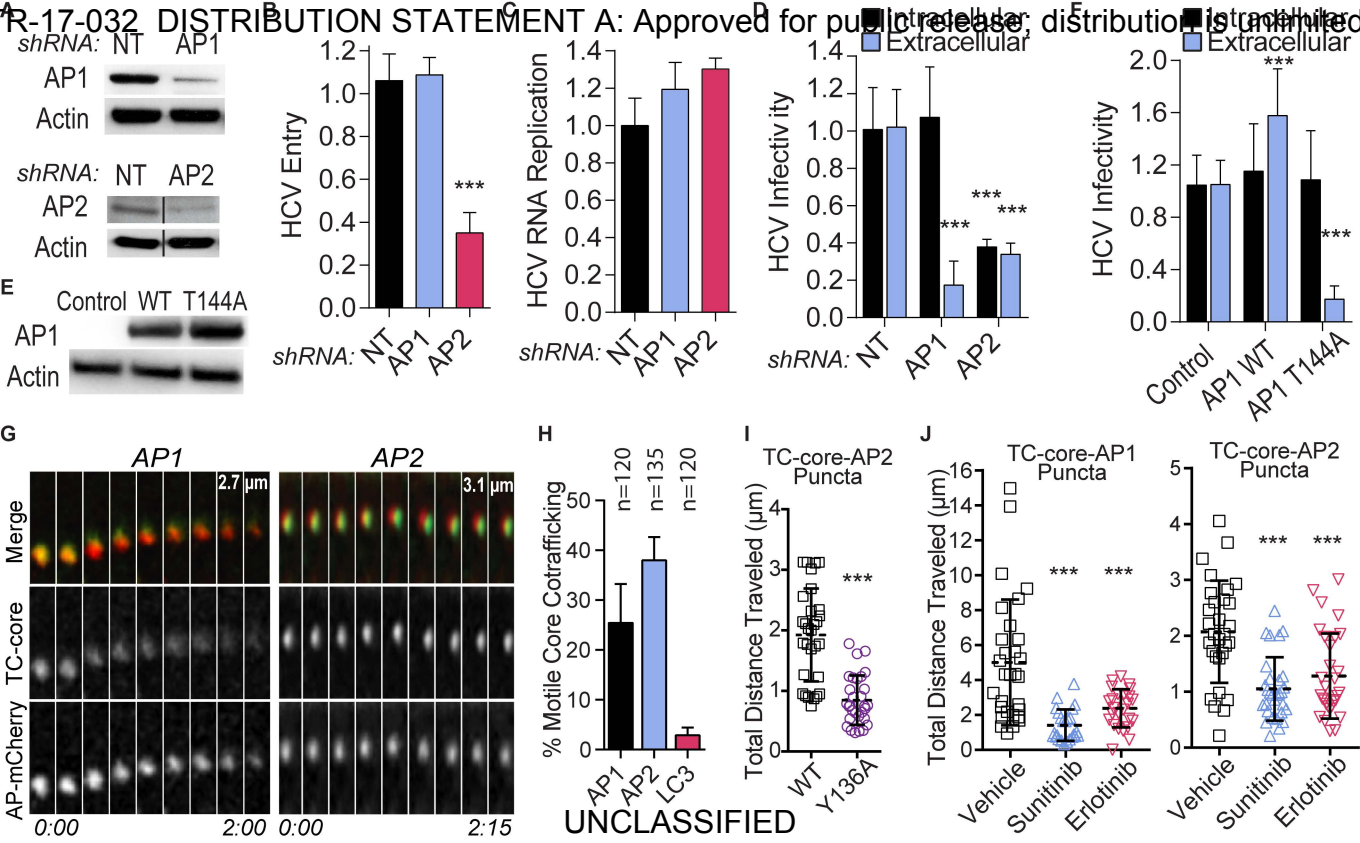
**Figure 6. Mechanisms underlying the antiviral effect of sunitinib and erlotinib in vitro and in vivo.** (A-C) Huh7 cells were treated with the inhibitors and monitored for DENV entry (A) at 6 hours post-infection, DENV RNA replication (B) post-induction of replication of DNA-

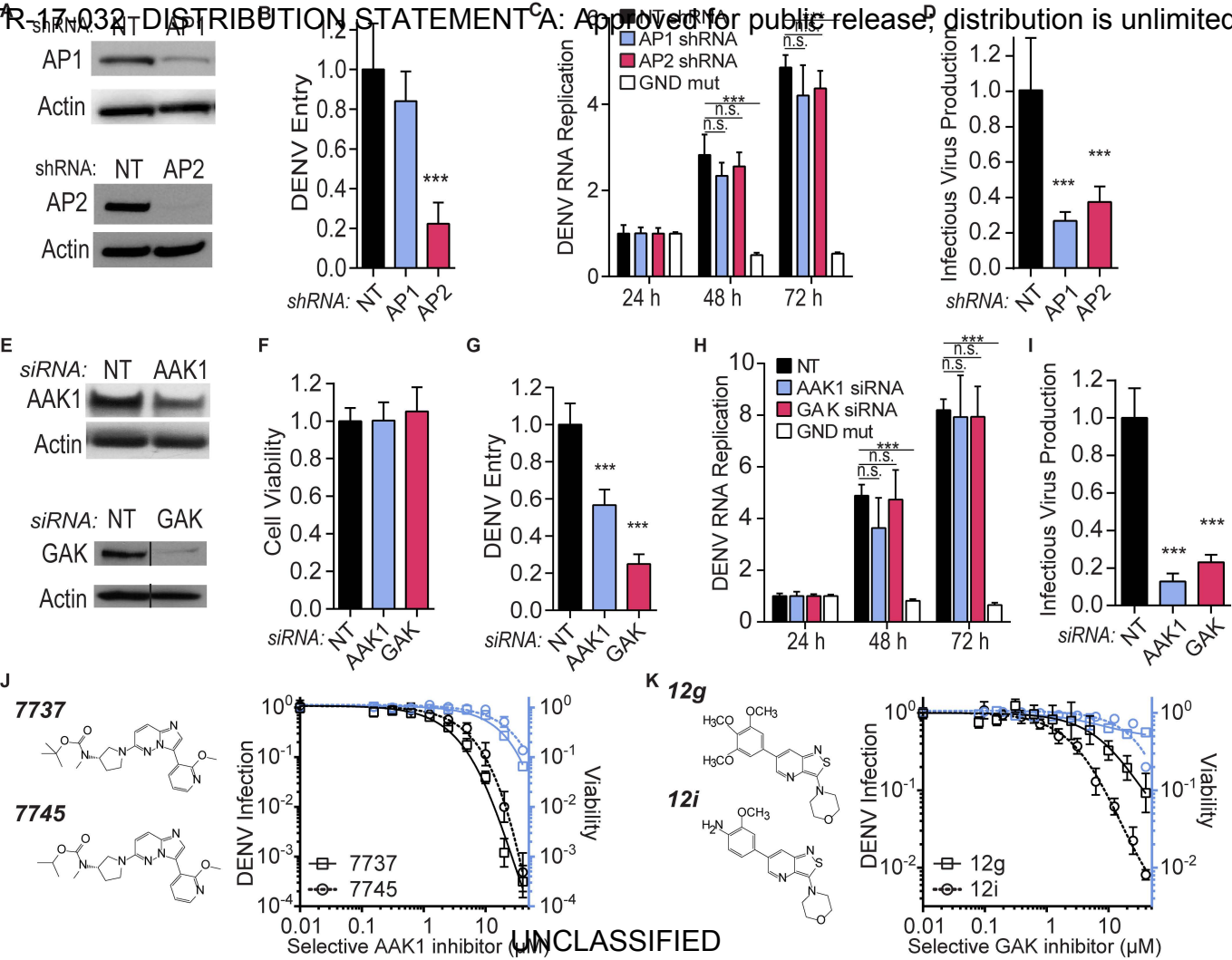
launched DENV replicon, and infectious virus production (C) at 48 hours post-electroporation with DENV RNA. SDM25N is an inhibitor of DENV RNA replication. (D) Effect of 1 hour treatment with erlotinib (E) and/or sunitinib (SM) on phosphorylation of AP2 in DENV-infected Huh7 cells measured by Western blotting. Arrow indicates ~50kDa. The ratio of phospho-AP2 (pAP2) to total AP2 was quantified. (E) Level of AP2 and actin expression measured by Western blot following lentiviral transduction with control or AP2 expressing constructs. (F) Rescue of DENV infection in the presence of inhibitors upon overexpression of WT or T156A AP2 vs. vector control measured by luciferase assays 48 hours post-infection.  $\mu$ M concentration of each inhibitor is noted on the x-axis. (G) Effect of 3 hour IP treatment with erlotinib (E) and/or sunitinib (SM) on phosphorylation of AP2 in liver tissue of AG-B6 mice measured by Western blotting and quantified as the ratio of pAP2 to total AP2. (H) DENV infection relative to NT control following siRNA-mediated knockdown of kinases targeted by sunitinib and erlotinib measured by luciferase assays at 48 hours and normalized to cell viability. Data in panels A, C, I are pooled from two independent experiments with 4-8 replicates each. Data in the other panels are representatives of two or more independent experiments. Panels B, F have at least 5 replicates each. \*\*\*  $p < 0.001$  relative to vehicle (B, H) or vector control (F) (two-tailed unpaired t-test). (N.s., non-significant).

**Figure 7. Model: AAK1/GAK in infection and as broad-spectrum antiviral targets.** Host kinases AAK1 and GAK regulate entry, assembly and/or release of multiple RNA viruses through phosphorylation of the membrane trafficking adaptors AP1 (pink) and AP2 (purple). Sunitinib, erlotinib and selective inhibitors of AAK1 and GAK disrupt these temporally distinct steps of the viral life cycle and act as broad-spectrum antivirals.

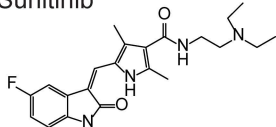
Family	Virus	Strain	Sunitinib EC50/CC50 ( $\mu$ M)	Erlotinib EC50/CC50 ( $\mu$ M)	Cells	Assay
Flaviviridae	HCV	J6/JFH	1.2/>10	0.6/>15	Huh7.5	Luciferase, FFA
	DENV1	276RKI, PRS41393	0.6/>10	1.9/>20	BHK-21	Plaque
	DENV2	TSV01, 429557, New Guinea C	0.51/11.5	2.5/>20- 6.5/>50	Huh7, BHK-21	Luciferase, plaque
	DENV3	Philippines/H87/1956	0.3/>10	1.3/>20	BHK-21	Plaque
	DENV4	BC287/97, H241	0.23/>10	3.9/>20	BHK-21	Plaque
	WNV	NY 99 3000.0259	0.55/>20	NE	MEF, Vero	FFA
	ZIKV	MR766	0.51/14.1	6.28/>30	Huh7	Plaque
Filoviridae	EBOV	Zaire	0.47/>10	12.9/>30 2.88/15	Huh7 Vero	Immuno-staining
Togaviridae	CHIKV	181/25	4.67/11.9	0.7/>30	Vero	Plaque
Arenaviridae	JUNV	Candid 1	4.8/10.4	1.7/>20	Vero	CPE
Retroviridae	HIV	NL4-3	0.8/>20	2/>20	HeLa/TZM-b1	Luciferase
Paramyxoviridae	RSV	A2	<0.12/12.5	<0.12/>30	Hep2	Immuno-plaque

**Table 1. Antiviral activity of sunitinib and erlotinib.** EC50, half maximal effective concentration; CC50, half maximal cellular cytotoxicity. Virus abbreviations: West Nile virus (WNV), chikungunya virus (CHIKV), Junin virus (JUNV), human immunodeficiency virus (HIV), Respiratory syncytial virus (RSV). NE, no effect. Each virus was tested as least twice with three or more technical replicates.





Sunitinib



Erlotinib

